Hansenula polymorpha Pex19p is essential for the formation of functional peroxisomal membranes

Otzen, M.; Perband, U.; Wang, D.Y.; Baerends, R.J S; Kunau, W.H.; Veenhuis, M; van der Klei, I.J.

Published in:
The Journal of Biological Chemistry

DOI:
10.1074/jbc.M314275200

Publication date:
2004

THE JOURNAL OF BIOLOGICAL CHEMISTRY
Vol. 279, No. 18, Issue of April 30, pp. 19181–19190, 2004
Printed in U.S.A.

Hansenula polymorpha Pex19p Is Essential for the Formation of Functional Peroxisomal Membranes*

Received for publication, December 29, 2003, and in revised form, February 22, 2004
Published, JBC Papers in Press, February 23, 2004, DOI 10.1074/jbc.M314275200

Marleen Otzen‡§, Uta Perband¶, Dongyuan Wang‡§, Richard J. S. Baerends‡‖, Wolf H. Kunau¶, Marten Veenhuis‡, and Ida J. Van der Klei‡§**

From the ‡Eukaryotic Microbiology, Groningen Biomolecular Sciences and Biotechnology Institute, University of Groningen, P. O. Box 14, 9750 AA Haren, The Netherlands and the ¶Abteilung für Zellbiochemie, Medizinische Fakultät, Ruhr-Universität Bochum, D-44780 Bochum, Germany

We have cloned and characterized the *Hansenula polymorpha PEX19* gene. In cells of a *pex19* disruption strain (Hp*pex19*), induced on methanol, peroxisome structures were not detectable; peroxisomal matrix proteins accumulated in the cytosol, whereas peroxisomal membrane proteins (PMPs) were mislocalized to the cytosol (Pex3p) and mitochondria (Pex14p) or strongly reduced to undetectable levels (Pex10p). The defect in peroxisome formation in Hp*pex19* cells was largely suppressed upon overproduction of HpPex3p or a fusion protein that consisted of the first 50 N-terminal amino acids of Pex3p and GFP. In these cells PMPs were again correctly sorted to peroxisomal structures, which also harbored peroxisomal matrix proteins. In *Saccharomyces cerevisiae pex19* cells overproduction of ScPex3p led to the formation of numerous vesicles that contained PMPs but lacked the major matrix protein thiolase. Taken together, our data are consistent with a function of Pex19p in membrane protein assembly and function.

Peroxisomes are single membrane-bound organelles that are present in virtually all eukaryotic cells. The biogenesis and maintenance of these organelles requires a fine-tuned orchestration of various processes, including among others protein sorting, membrane formation, and organelle fission. During the last 20 years the knowledge of the principles of peroxisome formation has rapidly expanded, and over 30 genes (designated *PEX* genes) have now been characterized that are involved in this process (for a recent review see Ref. 1).

Most *PEX* genes identified so far are required for sorting and translocation of peroxisomal matrix proteins across the peroxisomal membrane. Matrix proteins are synthesized in the cytosol and post-translationally imported into peroxisomes. Two peroxisomal targeting signals (PTS1 and PTS2)[1] are known that are recognized by soluble receptor proteins (Pex5p or Pex7p, respectively) that sort these proteins to the target organelle. In the case of peroxisomal membrane proteins (PMPs) several internal regions have been defined that contain peroxisomal targeting information (designated mPTS). However, consensus sequences, like those for matrix proteins, have not been defined yet. Pex19p has been proposed to play a role as a general mPTS receptor, but whether this is indeed the case is still a matter of debate (for a recent review see Ref. 1).

Observations that favor a function of Pex19p as mPTS-receptor include that, analogous to the PTS receptors for matrix proteins, in most organisms Pex19p has a dual location and is found in the cytosol and, to a minor extent, associated with peroxisomes (2, 3). Also in line with the putative mPTS receptor function is the observation that Pex19p physically interacts with multiple peroxisomal membrane proteins (3–5). Contrary to what may be expected for an mPTS receptor, Pex19p does not exclusively interact with the regions of PMPs that contain sorting information for the peroxisomal membrane. Moreover, mutations are known that affect targeting of PMPs to the peroxisomal membrane but not the interaction with Pex19p (2, 5).

The absence of peroxisomal membrane structures is the expected phenotype of cells lacking a general mPTS receptor. However, this phenotype may also be explained by a defect in the formation/assembly of the peroxisomal membrane, resulting in the absence of the target membrane for newly synthesized PMPs. *Saccharomyces cerevisiae pex19* mutants (6, 7) and human fibroblasts from patients with defects in *PEX19* lack peroxisomal membrane structures and display significantly reduced levels of PMPs that are mislocalized to the cytosol or other cell organelles (3). However, in *Pichia pastoris pex19* cells, small vesicular structures are observed that have been proposed to represent precursors of peroxisomes (2) and in *Yarrowia lipolytica pex19* cells structures are found that strongly resemble WT peroxisomes in size, shape, and protein composition (8). However, these organelles display a major defect in matrix protein import and reduced levels of PMPs.

To shed further light on a putative generalized function of Pex19p, we cloned the *Hansenula polymorpha PEX19* gene and analyzed its role in peroxisome biogenesis. In a constructed *H. polymorpha PEX19* disruption strain, peroxisomal structures were undetectable and PMPs were mislocalized. However, we observed that peroxisomes could be formed in the absence of HpPex19p upon overproduction of HpPex3p or the first 50 N-terminal amino acids of this protein, fused to GFP. These

* The costs of publication of this article were defrayed in part by the payment of page charges. This article must therefore be hereby marked "*advertisement*" in accordance with 18 U.S.C. Section 1734 solely to indicate this fact.

The nucleotide sequence(s) reported in this paper has been submitted to the GenBank™/EBI Data Bank with accession number(s) AF176708.

§ Supported by the Nederlandse Organisatie voor Wetenschappelijk Onderzoek.

‖ Current address: Molecular Genetics, Groningen Biomolecular Sciences and Biotechnology Institute, University of Groningen, P. O. Box 14, 9750 AA Haren, The Netherlands.

** To whom correspondence should be addressed. Tel.: 31-50-363-2179; Fax: 31-50-363-8280; E-mail: I.J.van.der.Klei@biol.rug.nl.

[1] The abbreviations used are: PTS1, -2, peroxisomal targeting signals 1 and 2; PMP, peroxisomal membrane protein; GFP, green fluorescent protein; eGFP, enhanced GFP; MES, 4-morpholineethanesulfonic acid; FCS, fluorescence correlation spectroscopy; AMO, amine oxidase; AO, alcohol oxidase; CAT, catalase; WT, wild type; DHAS, dihydroxyacetone synthase; mPTS, regions that contain peroxisomal targeting information.

TABLE I
Strains used in This study

Strains	Relevant properties	Reference
H. polymorpha		
NCYC495	Wild type, *ura3 leu1.1*	(45)
pex19::*URA3*	*PEX19* disruption strain, *leu1.1*	This study
pex19::P_{PEX19}*PEX19C286S*	*pex19* with one-copy integration of plasmid pHOR40	This study
pex19::P_{PEX3}*PEX19-GFP*	*pex19* containing the plasmid pHIPX6-PEX19-GFP	This study
pex19::P_{PEX3}*PEX19-GFP*::P_{AO}*DsRED-SKL*	*pex19*::P_{PEX3}*PEX19-GFP* with one-copy integration of plasmid pHIPX4-DsRED-SKL	This study
pex3::*LEU1.1 (ura3)*	*PEX3* disruption strain, *ura3*	(11)
NCYC495::P_{AO}*PEX3*$_{N50}$*-GFP (HF74)*	*NCYC495 w*ith one-copy integration of plasmid pFEM75	(19)
pex19::P_{AO}*PEX3*$_{N50}$*-GFP*	*pex19* with one-copy integration of plasmid pFEM75	This study
pex14::P_{PEX14}*PEX14-GFP*	NCYC495 with one-copy integration of plasmid pHIPX10-PEX14eGFPΔPstI	This study
pex19::*pex14*::P_{PEX14}*PEX14-GFP*	*pex19* with one-copy integration of plasmid pHIPX10-PEX14eGFPΔPstI	This study
pex19::*pex3*::P_{PEX3}*PEX3-GFP*	*pex19* with one-copy integration of plasmid pHOR46	This study
pex19::P_{AO}*PEX3*	*pex19* with multicopy integration of plasmid pHIPX4-PEX3	This study
pex3::P_{AO}*PEX19*	*pex3* with multicopy integration of plasmid pHIPX4-PEX19	This study
pex19::P_{PEX3}*MYC-PEX19*	*pex19* containing the plasmid pHIPX6-MYC-PEX19	This study
pex3::*pex19*::P_{AMO}*PEX3*$_{1–50}$*-GFP*	*pex3, pex19* with one-copy integration of plasmid pFEM167	This study
S. cerevisiae		
UTL-7A	WT	(46)
pex19	*PEX19* disruption strain	(6)
pex19 [Pex13p-tev-ProtA]	*pex19* producing Protein A tagged Pex13p	This study
pex19 [Pex13p-tev-ProA] + pTF14	*pex19* [Pex13p-tev-ProA] overproducing *PEX3* (*FOX3* promoter in YEp352)	This study
pex19 [Pex13p-tev-ProA] + pTF15	*pex19* [Pex13p-tev-ProA] overproducing *PEX3* (*CTA1* promoter in YEp352)	This study
P. pastoris		
P. pastoris SKF13	*PEX19* disruption strain	(2)

data suggest that *H. polymorpha* Pex19p is not essential for sorting of PMPs. Also in *S. cerevisiae pex19* cells peroxisomal membranes could be reintroduced by overproduction of ScPex3p. The details of this work are included in this report.

EXPERIMENTAL PROCEDURES

Organisms and Growth—The *H. polymorpha*, *P. pastoris*, and *S. cerevisiae* strains used in this study are listed in Table I. *H. polymorpha* cells were cultivated at 37 °C, *P. pastoris* and *S. cerevisiae* at 30 °C. Yeast cells were grown on 1% yeast extract, 1% peptone, and 1% glucose, selective minimal media containing 0.67% yeast nitrogen base without amino acids (Difco) or mineral media (9) supplemented with glucose (0.5%), methanol (0.5%), or glycerol (0.5%) as carbon source and methylamine (0.25%) or ammonium sulfate (0.25%) as nitrogen source. *S. cerevisiae* cells were grown on yeast nitrogen base containing 0.1% oleic acid, 0.05% Tween 40, 0.1% yeast extract, and 0.1% glucose. When required, amino acids or uracil were added to a final concentration of 30 μg/ml. For growth on agar plates, the media were supplemented with 1.5% agar. *Escherichia coli* was grown on LB medium (10), supplemented with ampicillin (100 μg/ml), or kanamycin (50 μg/ml) when required.

Molecular Techniques—Standard recombinant DNA techniques were carried out essentially according to Sambrook *et al.* (10). Primers used for polymerase chain reactions in this study are listed in Table II. Transformation of *H. polymorpha* cells and site-specific integration of single or multiple copies of plasmid DNA in genomic *AOX*-, *PEX3*-, or *AMO*-locus was performed as described previously (11–15). For the replacement of the wild type *PEX14* gene with the *PEX14-GFP* fusion gene, the plasmid pHIPX10-PEX14eGFPΔPstI was linearized with SalI. The plasmid pHOR50 was linearized using BsgI for the integration into the *PEX19*-locus.

Isolation and Characterization of the H. polymorpha PEX19 Gene—*P. pastoris pex19* (SKF13) was transformed with an *H. polymorpha* genomic library in the *P. pastoris* vector pYM8 (16). Histidine prototrophic transformants were screened for the ability to grow on methanol. From a selected positive strain the plasmid, designated pHP19-5, was rescued and transformed to *E. coli* dH5α. To facilitate sequencing, restriction analysis and construction of subclones, a 2.9-kb DNA fragment obtained from pHP19-5 was subcloned as an NheI-HindIII fragment into HindIII-XbaI-digested phagemid pBluescript II KS$^+$ (pBSII KS$^+$, Stratagene Inc., San Diego, CA), resulting in pHOR28. Double strand sequencing was carried out on an ABI 373A automatic sequencer (Applied Biosystems Inc.) using the *Taq* Dye Deoxy Terminator Cycle Sequencing kit. For DNA and amino acid sequence analysis the PC-GENE™ program release 6.70 (IntelliGenetics, Mountain View, CA) was used. The BLASTN algorithm (17) was used to search the GenBank™ data base (Release 91.0, October 15, 1995) for DNA, and protein sequences showing similarity to the Hp*PEX19* gene and its translation product. The nucleotide sequence of Hp*PEX19* was deposited at GenBank™ and was assigned accession number AF176708.

PEX19 Disruption in H. polymorpha—For disruption of the complete *H. polymorpha PEX19* gene the *H. polymorpha URA3* gene was used (18). The *URA3* was isolated as a BglII, PstI fragment and ligated between the two flanking regions of the *H. polymorpha PEX19* gene. These regions were obtained by PCR on pHOR28 using primers RB12 and RB13 containing the sequence upstream the start codon, digested with BglII and the primers −40 uni × RB11, containing the sequence downstream the stop codon, digested with PstI. This fragment was used to transform *H. polymorpha* NCYC495 *leu1.1 ura3.* Methanol utilization-deficient (Mut$^-$) colonies were selected. Correct integration was analyzed by Southern blotting using the ECL direct nucleic acid labeling and detection system (Amersham Biosciences, Arlington Heights, IL).

Plasmid Constructions—Expression plasmids pHIPX4-PEX3 (14), pHIPX4-PEX3$_{N50}$GFP (pFEM75) (19), pHOR46 (15), and pHIPZ5-PEX3$_{N50}$GFP (pFEM167) (20) have been described before. pHIPX4-PEX19 (pHOR32) was constructed as follows. Using PCR and primers RB16 and RB17 a BamHI site was introduced upstream the start codon, and a SalI site downstream the stop codon of the *H. polymorpha PEX19* gene. These sites were used to clone the *PEX19* gene into a BamHI-SalI-digested pHIPX4 (21).

For localization of HpPex19p, *MYC-PEX19* was expressed under control of the *PEX3* promoter. For this plasmid pHIPX6-MYC-PEX19, *MYC-PEX19* was amplified using the primers RB17 × RB26, resulting in a product containing an in-frame fusion between the *MYC* tag and the *PEX19* gene. This PCR product was then digested with BamHI and SalI and ligated into the BamHI-SalI digested pHIPX6 (14). A second construct, used for the localization of HpPex19p, included a hybrid gene under control of the *PEX3* promoter encoding a HpPex19p.GFP fusion protein (pHIPX6-PEX19-GFP). The green fluorescent protein (GFP, Clontech) was fused to the C terminus of Pex19p. The *PEX19* gene was amplified using primers 19GFP-start and 19GFP-stop, resulting in a product lacking the stop codon of the *PEX19* gene. This PCR product was then digested with HindIII and ligated into pANL31 (22), resulting in plasmid pHIPZ-PEX19-GFP, containing an in-frame fusion of the whole *PEX19* gene fused to the eGFP gene. This product was subsequently restricted with BamHI and SmaI, and ligated into a BamHI, SmaI-digested pHIPX6.

To identify peroxisomes, the gene encoding DsRed-T1-SKL was expressed under control of the alcohol oxidase promoter (P_{AOX}). A DNA fragment encoding an in-frame fusion of DsRED-T1 and SKL was obtained by PCR using primers DsRed-1 and DsRed-2, and a plasmid

TABLE II
Primers used in This study

Primers	Sequence
RB12	CCC AGA TCT TGA AAA GTT TCT AAA CCC
RB13	GGG GTC GAC TTT TGC AAG TGA TTC
RB11	GGG CTG CAG TTA TGG TTA ATA TGA GCG
−40 uni (Stratagene)	GTT TTC CCA GTC ACG AC
RB16	TAA GGA TCC ATG AGC GAG AAA AAG TCC G
RB17	CTT TGT CGA CCT ATG TTT GTT TGC AAG TG
RB18	CCC TGT CGA CCT ATG TTT GTT TAC TAG TGT CTT CCA GTT C
RB26	GGG GGA TCC ATG GAG CAG AAG TTG ATT TCT GAG GAA GAC TTG AGC GAG AAA AAG TCC G
RB36	GAG GCG GCC GCG GTT CTT GTG GAT TCG AC
RB37	GGG GGA TCC TTA TGG TTA ATA TGA GCG
19GFP-start	CCC AAG CTT ATG AGC GAG AAA AAG TCC G
19GFP-stop	GTG TTT GTT TGC AAG TGT CTT CC
DsRED-1	AGA GGA TCC ATG GCC TCC TCC GAG GAC G
DsRED-2	AGA GTC GAC TTA CAG CTT CGA CTT GTA CAA TTC GTC CAT ACC

containing DsRed-T1 (23) in-frame fused to HDEL containing a spacer peptide THGMDELYK, kindly donated by B. Glick. The PCR product was digested with BamHI and SalI and subsequently ligated in pHIPX4 digested with BamHI and SalI, resulting in plasmid pHIPX4-DsRed-T1-SKL.

For the construction of a gene encoding Myc-Pex19p containing an amino acid substitution in the farnesylation site, plasmid pHOR50 was constructed. For this purpose plasmid pHIPX13, containing the *PEX19* promoter, was constructed by amplification of the *PEX19* promoter using primers RB36 and RB37. The PCR product was then ligated as a NotI-BamHI fragment in pHIPX4, digested with NotI and BamHI. For the plasmid pHOR40 the *PEX19* gene was amplified using primers RB26 and RB18, resulting in a product containing an N-terminal myc-tagged HpPex19p with an amino acid substitution (C286S) at the C terminus. The PCR product was then digested with BamHI and SalI and inserted into BamHI-SalI-digested pHIPX13.

For the localization of HpPex14p, a plasmid encoding a fusion protein consisting of HpPex14p containing GFP at the C terminus was constructed. This was performed by digestion of pHIPX10-PEX14eGFP, kindly donated by M. Komori (Osaka Prefecture University, Osaka, Japan), with PstI. This resulted in plasmid pHIPX10-PEX14eGFPΔPstI.

S. cerevisiae strains, containing genomic copies of a hybrid Sc*PEX13* gene encoding ScPex13p fused to the tobacco etch virus protease cleavage site followed by a Protein A tag (−TEV-ProtA) were obtained by transforming haploid yeast cells with the corresponding PCR product according to Knop *et al.* (24). Sc*pex19* strains overproducing Sc*PEX3* were obtained by transforming Sc*pex19* with plasmid pTF14 (expression plasmid containing *ScPEX3* under control of the *FOX3* promoter) or pTF15 (expression plasmid containing *PEX3* under control of the *CTA1* promoter). Cloning strategies and sequences of primers used to make pTF14 and pTF15 are available upon request.

Biochemical Methods—Crude extracts of *H. polymorpha* cells were prepared as described by Baerends *et al.* (19). Subcellular fractionation of *H. polymorpha* cells was performed as detailed before (25) except that a modified sucrose gradient was used consisting of 4 ml of 65%, 9 ml of 50%, 9 ml of 40%, and 4 ml of 35% (w/v)-sucrose in buffer B (5 mM MES, 0.1 mM EDTA, 1 mM KCl, pH 5.5). Flotation centrifugation of *H. polymorpha* fractions was carried out according to Goodman *et al.* (26).

S. cerevisiae cells were fractionated by differential centrifugation. Cells were converted to spheroplasts using zymolyase (20 units/g cells). Spheroplasts were washed three times in a solution containing 1.2 M sorbitol and homogenized in 0.6 M sorbitol in 5 mM MES, pH 6.0, supplemented with 0.5 mM EDTA and 1 mM KCl (fractionation buffer). Intact cells and nuclei were removed from the homogenate by two centrifugation steps at 600 × *g* for 10 min. The resulting post nuclear supernatant (T) was further fractionated by differential centrifugation resulting in a 25,000 × *g* pellet, 25,000 × *g* supernatant, 100,000 × *g* pellet, and a 100,000 × *g* supernatant. Pellet fractions were resuspended in fractionation buffer. Equivalent volumes of these fractions were analyzed by SDS-PAGE and immunoblotting.

Enzyme activities of alcohol oxidase (27) and cytochrome *c* oxidase (28) were assayed as described. Protein concentrations were determined using the Bio-Rad Protein Assay system (Bio-Rad GmbH, Munich, Germany) using bovine serum albumin as standard.

SDS-PAGE (29) and native gel electrophoresis (30) was carried out as described. Western blotting was performed as detailed by Kyhse-Andersen (31). Blots were decorated using specific antibodies against various proteins using either the Protoblot immunoblotting system (Promega Biotec) or a BM Chemiluminescence Western blotting kit (Roche Applied Science, Almere, The Netherlands). Polyclonal antibodies against HpPex19p were raised in rabbit, using synthetically synthesized HpPex19p peptides (amino acids 1–15 and 194–208).

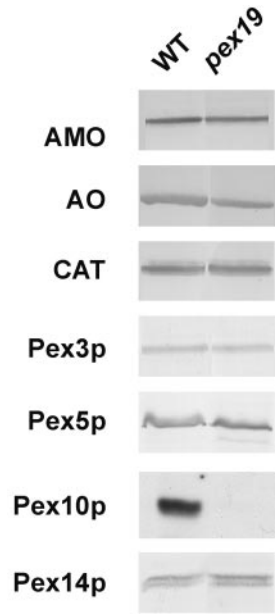

FIG. 1. **Levels of peroxisomal matrix proteins and peroxins in chemostat-grown *H. polymorpha pex19* cells relative to wild type levels.** Western blots were prepared of crude extracts and decorated with antibodies against *H. polymorpha* amine oxidase (*AMO*), alcohol oxidase (*AO*), catalase (*CAT*), Pex3p, Pex5p, Pex10p, and Pex14p. The levels of all proteins were similar in both strains, except for Pex10p, which was below the level of detection in Hp*pex19* cells.

Fluorescence Correlation Spectroscopy—HpPex19.GFP present in soluble and membrane fractions of methanol-grown *H. polymorpha pex19*::P_{PEX3}*PEX19-GFP* cells was analyzed by fluorescence correlation spectroscopy (FCS). *H. polymorpha* cells that did not produce HpPex19.GFP were used as controls. Cells were harvested by centrifugation, resuspended in buffer A (50 mM Tris-HCl, pH 7.0, containing 300 mM NaCl, 10% glycerol, 0.1 mM phenylmethylsulfonyl fluoride, and Complete™ protease inhibitor mixture), and broken using a French pressure cell. The cell lysate was centrifuged for 1 h at 100,000 × *g* (4 °C) and resulted in a soluble fraction (designated S), which was used for FCS measurements. The pellet (P) was washed once in buffer A and subsequently resuspended in buffer A containing 1% digitonine to solubilize membrane proteins, followed by centrifugation at 100,000 × *g* for 1 h (4 °C). The supernatant, representing the solubilized membrane protein fraction (designated P), was also used for FCS measurements.

The ConfoCor2 (Zeiss the Netherlands BV, Weesp, The Netherlands), a dual channel system based on a Zeiss Axiovert 100M inverted microscope, was used to acquire fluorescence fluctuation data. The system is equipped with an argon ion laser line of 488 nm and a 40 × 1.2 water immersion apochromatic objective and is controlled by AIM3.1 software (EMBL Heidelberg, Germany). The system was calibrated by optimiz-

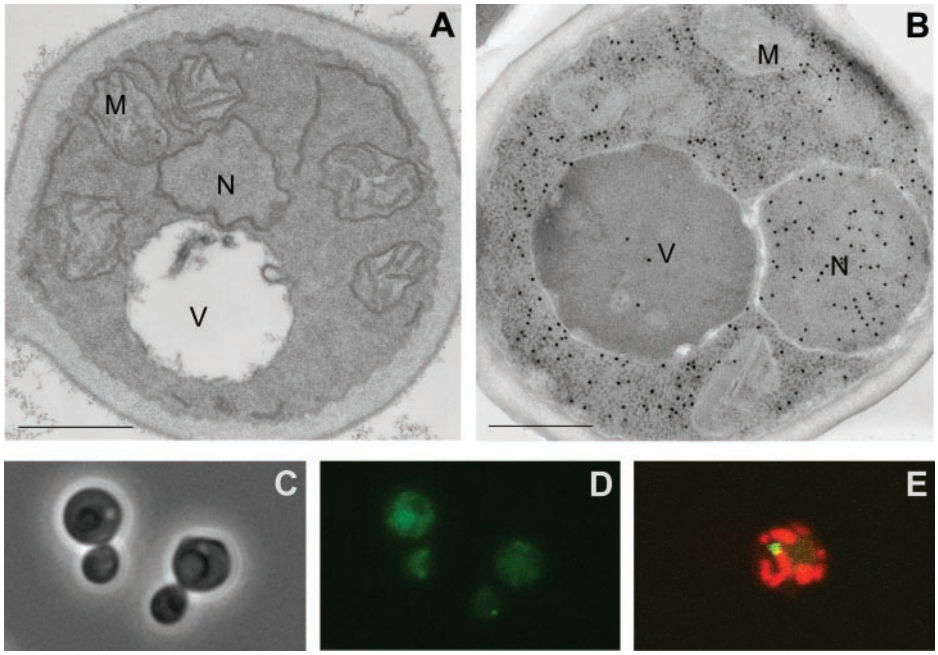

FIG. 2. **Morphological analysis of Hp*pex19* cells.** In ultrathin sections of $KMnO_4$-fixed, chemostat-grown cells (*A*) peroxisomal structures were not detectable. Immunolabeling experiments revealed that the matrix proteins AO and DHAS were mislocalized to the cytosol and nucleus (*B*, AO; DHAS not shown). Fluorescence microscopy showed that in Hp*pex19* cells HpPex3p.GFP is localized to the cytosol (*D*). *C*, bright-field picture. Analysis by confocal laser scanning microscopy (*E*) indicated that HpPex14p.GFP (*green*) is present in a single spot on mitochondria (visualized in *red* by MitoTracker). In this latter figure the cell is not visualized. The *bar* in *A* and *B* represents 0.5 μm. *N*, nucleus; *M*, mitochondrion; *V*, vacuole.

ing the position of the pinhole and the correction ring of the objective lens using a solution of 5 nM Alexa Fluor 488 (Molecular Probes, Leiden, The Netherlands). Samples were measured in 96-well plates. Autocorrelation traces were acquired during 10 or 20 s at room temperature and repeated 20 times. Autocorrelation curves were globally analyzed to multicomponent three-dimensional Brownian motion models, which included triplet kinetics using the FCS data processor 1.3 software (the Scientific Software Technologies Center of Belarusian State University, Belarus) as detailed before (32–34).

Microscopy—Fluorescence microscopy was performed as described before (19). Confocal laser scanning microscopy on living cells was carried out using a Zeiss LSM 510 META-NLO confocal laser scanning microscope (Zeiss, the Netherlands BV) equipped with a Zeiss plan-apochromatic 63× numerical aperture 1.4 objective. GFP fluorescence was analyzed by excitation of the cells with a 488-nm argon/krypton laser, and fluorescence was detected by a BP 500–550 Photo Multiplier Tube (PMT). Whole cells were treated for 10 min at 37 °C with 50 μg/ml Hoechst 33258 (Sigma, Nieuwegein, The Netherlands) to stain nuclei. Mitochondria were stained by incubation of intact cells for 30 min at 37 °C with 0.5 μg/ml MitoTracker Red Cm-H_2XROS (Molecular Probes) followed by extensive washing with medium.

Cells incubated with Hoechst 33258 were analyzed using excitation at 760 nm (Ti-Sapphire laser) and detection by a BP 435- to 485-nm PMT. Cells treated with MitoTracker were excited at 543 nm (He laser), and fluorescence was detected using a BP 565- to 615-nm PMT.

Whole cells were fixed and prepared for electron microscopy and immunocytochemistry as described previously (35). Immunolabeling was performed on ultrathin sections of Unicryl-embedded cells, using specific antibodies against various proteins and gold-conjugated goat-anti-rabbit antibodies, or goat-anti-mouse antibodies (35).

RESULTS

Cloning of the H. polymorpha PEX19 Gene—A *P. pastoris PEX19* disruption strain was functionally complemented by transformation with an *H. polymorpha* genomic library. The plasmid, recovered from complemented *P. pastoris* cells, contained an open reading frame encoding a protein with high homology to Pex19 proteins (*e.g.* 41% identity to *P. pastoris* Pex19p). Also, it contained the typical Pex19p farnesylation site (-CKQT) at the extreme C terminus. To further substantiate that the cloned gene represented *H. polymorpha PEX19*, a disruption strain (Hp*pex19*) was constructed. Cells of this strain were unable to grow on methanol, which is characteristic for *H. polymorpha PEX* mutants (36). Based on these findings we concluded that the cloned gene represented Hp*PEX19*. The sequence of the complementing DNA fragment was deposited at GenBank™ (accession number AF176708).

To characterize the peroxisome phenotype of Hp*pex19* cells in detail, the cells were grown in a glucose-limited chemostat using choline as sole nitrogen source. These conditions result in massive peroxisome proliferation and strong induction of peroxisome matrix and membrane proteins in WT cells (37). Western blot analysis of crude cell extracts revealed that the levels of the matrix proteins alcohol oxidase (AO), catalase (CAT), and amine oxidase (AMO) were similar in WT and Hp*pex19* cells (Fig. 1). Also the peroxisomal membrane proteins (PMPs) HpPex3p and HpPex14p as well as the PTS1 receptor Pex5p were detected at similar levels in both strains. However, the level of the integral PMP HpPex10p was strongly reduced in Hp*pex19* cells and below the limit of detection.

Electron microscopy studies revealed that peroxisomes or peroxisomal remnant structures (ghosts) were not detectable in Hp*pex19* cells (Fig. 2*A*). Immunocytochemistry demonstrated that the matrix proteins AO, CAT, AMO, and dihydroxyacetone synthase (DHAS) were mislocalized to the cytosol (see Fig. 2*B* for AO). Using specific antisera against PMPs, α-HpPex3p-specific labeling was observed on the cytosol, whereas α-HpPex14p-dependent labeling was confined to discrete spots on mitochondrial profiles (data not shown).

The presence of cytosolic HpPex3p and the localization of HpPex14p at mitochondria was confirmed by fluorescence microscopy (Fig. 2, *C–E*). To this purpose Hp*pex19* strains were constructed in which the authentic Hp*PEX3* gene was replaced by an Hp*PEX3.GFP* hybrid gene (*pex19.pex3*::P_{PEX3}*PEX3-GFP*), or the Hp*PEX14* gene was replaced by an Hp*PEX14.GFP* hybrid gene (*pex19.pex14*::P_{PEX14}*PEX14.GFP*). Both fusion proteins are fully functional, because they functionally complement the *pex* phenotype of *H. polymorpha pex3* (15) and *pex14* cells, respectively (data not shown).

The mislocalization of HpPex3p and HpPex14p were also demonstrated by biochemical analyses using sucrose density centrifugation of post-nuclear supernatants prepared from chemostat-grown cells (Fig. 3*A*). Analysis of the various fractions obtained demonstrated that no protein peak was observed at a density of 52% sucrose, the position where peroxisomes of WT cells normally sediment (25). AO, HpPex3p, and minor amounts of HpPex14p were present in the upper fractions of the gradient, where soluble cytosolic proteins are located, whereas the bulk of HpPex14p and a minor amount of HpPex3p

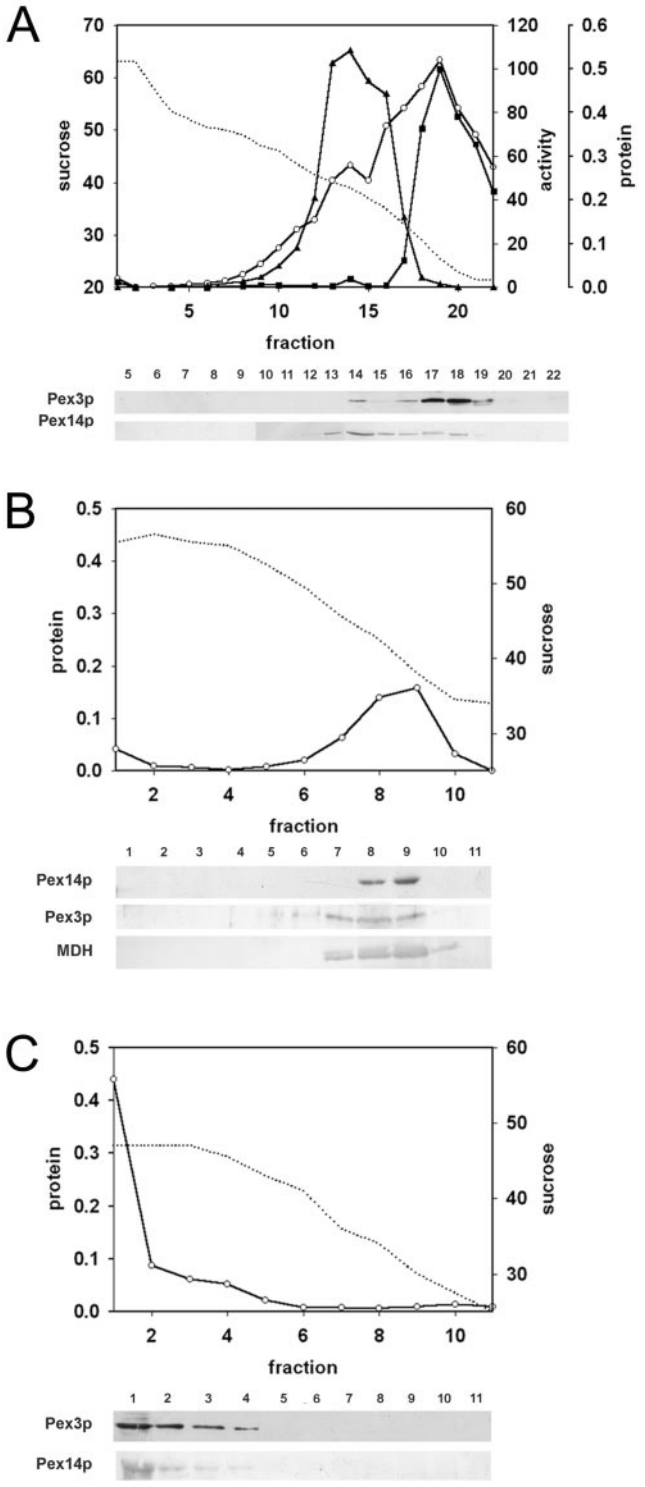

FIG. 3. **Subcellular fractionation of Hp*pex19*::*pex14*::P_{PEX14}-*PEX14.GFP* cells.** A postnuclear supernatant prepared from chemostat-grown cells was subjected to sucrose density centrifugation. *A*, protein (○) and sucrose (*dotted line*) concentrations, mitochondrial cytochrome *c* oxidase activities (▲) peroxisomal AO activities (■). The *panel below* shows Western blots of *fractions 5–22* decorated with the indicated antibodies. HpPex3p and HpPex14p have different locations. *B*, a flotation analysis of the pooled HpPex14p peak fractions of the sucrose gradient (*fractions 13–15*); *C*, the flotation analysis of the fractions (*17* and *18*), which contained the bulk of HpPex3p. The fractions of the flotation gradients were analyzed by Western blotting using the indicated antibodies. *MDH*, mitochondrial marker protein malate dehydrogenase. Protein concentrations are indicated as $mg.ml^{-1}$, sucrose concentrations as % (w/w). Enzyme activities are expressed as percentages of the activity in the peak fractions, which were arbitrarily set to 100. For Western blots equal portions of the fractions were loaded per lane.

co-fractionated with mitochondria (*fractions 13–15*, Fig. 3*A*). To further substantiate that the bulk of the HpPex14p is bound to mitochondria, whereas HpPex3p is predominantly soluble, their respective peak fractions of the sucrose gradient were subjected to flotation centrifugation. Upon flotation centrifugation of the HpPex14p peak fractions (*fractions 13–15*, Fig. 3*B*), HpPex14p protein migrated to the upper part of the gradient to the same position as the mitochondrial marker protein malate dehydrogenase (38). The minor amounts of HpPex3p present in these fractions behaved similarly. These results are consistent with the microscopy findings that bulk of the HpPex14p is mislocalized to mitochondria in Hp*pex19* cells. In identical experiments using the HpPex3p peak fractions (*fractions 17* and *18*, Fig. 3*A*), HpPex3p remained at the bottom of the gradient upon flotation centrifugation (Fig. 3*C*), indicating that the bulk of this protein was not membrane-bound.

Overproduction of HpPex3p Restores Peroxisome Formation in Hppex19 Cells—The mislocalization of PMPs in Hp*pex19* cells may have multiple causes and be the result of a defect in PMP sorting or alternatively caused by the absence of the normal target membrane. To distinguish between the two latter possibilities we aimed to introduce peroxisomal membrane vesicles in Hp*pex19* cells. This approach was based on earlier findings in Hp*pex3* cells that also lack peroxisomal membrane structures, but in which peroxisomal membrane vesicles are formed upon production of a fusion protein consisting of the first 50 amino acids of HpPex3p and GFP (HpPex3p_{N50}.GFP) (20). This N-terminal part of HpPex3p contains peroxisomal targeting information. Hence, when HpPex3p_{N50}.GFP is produced in wild type cells, this protein is properly sorted to peroxisomes (20) (Fig. 4*A*).

First, we analyzed whether the formation of peroxisomal membrane vesicles in Hp*pex3* cells was dependent on the function of HpPex19p. To this end, we produced HpPex3p_{N50}.GFP under control of the amine oxidase promoter (P_{AMO}) in a constructed *pex3.pex19* double disruption strain. As shown in Fig. 4*C*, fluorescent spots were detected in these cells in the vicinity of the nuclei, similar to that observed in Hp*pex3* cells synthesizing HpPex3p_{N50}.GFP and representing membrane vesicles (20). This suggests that HpPex19p is not required for the formation of these membrane vesicles. Subsequently, we produced HpPex3p_{N50}.GFP in Hp*pex19* cells. Methanol-induced cells of this strain showed relatively large, bright fluorescent spots when observed by fluorescence microscopy (Fig. 4*B*). Electron microscopic analysis of $KMnO_4$-fixed cells demonstrated that these cells contained peroxisome-like structures that were reduced in size relative to WT peroxisomes (data not shown). Immunocytochemistry revealed that the HpPex3p_{N50}.GFP fusing protein was localized at the membranes of these structures together with HpPex3p and HpPex14p (Fig. 5). In similar experiments using antibodies against the major peroxisomal matrix proteins, we found that these structures contained a significant fraction of AO and DHAS but not CAT protein (Fig. 5).

Cell fractionation (Fig. 6) and flotation experiments (data not shown) confirmed that in these cells the PMPs HpPex3p and HpPex14p co-sedimented again and were membrane-associated. However, as in *Hppex19*, the level of HpPex10p was below the level of detection (Fig. 6*B*).

When instead of Pex3p_{N50}.GFP full-length HpPex3p was overproduced in *Hppex19* (*pex19*::P_{AOX}*PEX3*), peroxisomal structures were also detected in the cells (data not shown). Partial suppression of the peroxisome-deficient phenotype was not observed when Pex19p was overproduced in Hp*pex3* cells (*pex3*::P_{AOX}*PEX19*). In such cells peroxisomes or peroxisomal remnant structures could not be detected (data not shown). These data are consistent with the hypothesis that mislocal-

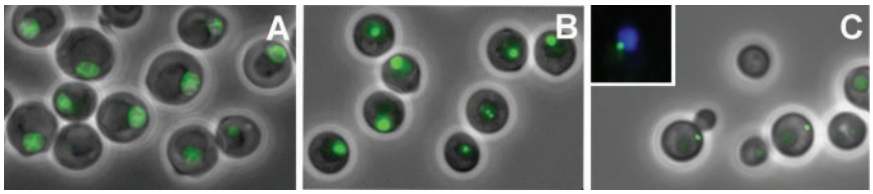

FIG. 4. **Localization of HpPex3p$_{N50}$.GFP by fluorescence microscopy.** HpPex3p$_{N50}$.GFP was synthesized in WT (*A*), Hp*pex19* (*B*), and the *pex3 pex19* double mutant (*C*). Overlays of bright-field and fluorescence pictures are shown. In WT control cells, HpPex3p$_{N50}$.GFP is sorted to the peroxisomal membrane, resulting in fluorescent spots that consist of clusters of peroxisomes. In Hp*pex19* cells (*B*) and cells of the *pex3 pex19* double mutant (*C*), fluorescent spots are also evident. These spots are generally formed in the vicinity of the nucleus, which is visualized by Hoechst 33258 (*blue*; *C*, *inset*).

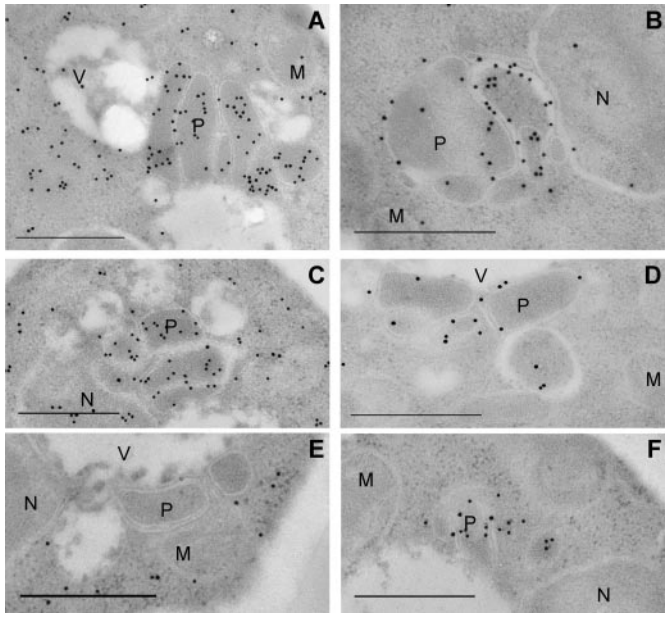

FIG. 5. **Peroxisome structures are formed in Hp*pex19* cells producing Pex3p$_{N50}$.GFP.** Ultrathin sections of chemostat-grown Hp*pex19*::P_{AOX}*PEX3*$_{N50}$*.GFP* cells were used for immunolabeling experiments. These experiments revealed that the peroxisomal matrix protein AO (*A*) and DHAS (*C*) are present both in peroxisomes and in the cytosol, whereas peroxisomal catalase was fully mislocalized to the cytosol (*E*). Anti-GFP labeling revealed that HpPex3p$_{N50}$.GFP was present at the peroxisomal membranes (*B*), where HpPex3p (*D*) and HpPex14p (*F*) are located as well. The *bars* represent 0.5 μm. *P*, peroxisome; *M*, mitochondrion; *N*, nucleus; *V*, vacuole.

ization of HpPex3p and HpPex14p in *pex19* cells is most likely due to the absence of their normal target membrane rather than the result of a defect in PMP targeting.

Overproduction of ScPex3p in S. cerevisiae pex19 Cells Results in Peroxisomal Membrane Formation—To analyze whether the data depicted above are unique for *H. polymorpha* or also valid in other yeast, we overproduced full-length ScPex3p in an *S. cerevisiae PEX19* disruption strain (Sc*pex19*) (6). To this end a strain was constructed that contained Sc*PEX3* under control of a strong promoter (P_{FOX3} or P_{CTA1}). Electron microscopy revealed the presence of high numbers of vesicular structures in these cells (Fig. 7, *B* and *C*) that were absent in Sc*pex19* controls (Fig. 7*A*). These membranes contained ScPex3p as evident from immunocytochemistry (Fig. 7*D*), but not thiolase (not shown), which remained mislocalized in the cytosol of these cells.

The stability and localization of PMPs in the *S. cerevisiae* strains was also analyzed biochemically. To facilitate the detection of ScPex13p, strains producing an ScPex13p-Protein A fusion protein were used (24). Cell fractionation experiments revealed that in WT controls ScPex13p and ScPex3p were predominantly present in the organellar pellet fractions (25,000 $\times$ *g* pellet, Fig. 8) upon differential centrifugation of a postnuclear supernatant. In the absence of ScPex19p the levels of both proteins were strongly reduced and below the level of detection at normal exposure times of the Western blots. Using prolonged exposure times (Fig. 8, *asterisk*), it became evident that most of the remaining ScPex3p and ScPex13p fractions were soluble in Sc*pex19* cells (25,000 $\times$ *g* and 100,000 $\times$ *g* supernatants, Fig. 8*A*), but became pelletable again upon overproduction of ScPex3p (25,000 $\times$ *g* pellet, Fig. 8). At the same time the level of ScPex13p increased again, suggesting that this PMP was stabilized upon overproduction of ScPex3p. Flotation analysis confirmed that ScPex3p and ScPex13p were indeed membrane-bound again in *Scpex19* cells overproducing ScPex3p (data not shown).

HpPex19p.GFP Localization—To analyze the subcellular location of HpPex19p, polyclonal antibodies were raised against HpPex19p. Using these antibodies, we were unable to detect a cross-reacting protein band on Western blots prepared from crude extracts of methanol-grown *H. polymorpha* WT cells. We therefore constructed a strain that expressed the *PEX19* gene under control of the weak *PEX3* promoter. A Myc tag was fused to the N terminus of HpPex19p to be able to detect the protein with commercially available monoclonal anti-Myc antibodies as well (strain *pex19*::P_{PEX3}*Myc-PEX19*). Cells of this strain grew normally on methanol, indicating that the Myc-tagged Pex19p was functional. In crude extracts of methanol-grown cells of this strain a protein band with an apparent molecular mass of 47 kDa was detected using anti-Pex19p (Fig. 9*A*) or anti-myc (not shown) antibodies. However, in fractions of sucrose gradients prepared from these cells, the protein remained undetectable, probably because it is unstable or susceptible to proteolytic degradation.

We then aimed to localize HpPex19p by fluorescence microscopy. The constructed strain *pex19*::P_{PEX3}*PEX19-GFP* was capable of growing on methanol and formed normal peroxisomes, indicating that HpPex19p.GPF is functional (data not shown). Fluorescence microscopy of methanol-grown cells of this strain revealed that fluorescence was present in the cytosol and enhanced at the periphery of peroxisomes, which were characterized by red fluorescence due to the incorporation of the red fluorescent protein DsRed (*DsRed-SKL*, Fig. 9*B*).

HpPex19p.GFP Is a Component of Large Complexes Both in the Cytosol and at Membranes—Whether HpPex19p is an mPTS receptor that binds to newly synthesized PMPs in the cytosol or functions as a chaperone is still a matter of debate. To analyze the presence of putative PMP-HpPex19p protein complexes, we analyzed HpPex19p.GFP by fluorescence correlation spectroscopy (FCS) and native gel electrophoresis in soluble and membrane fractions of crude cell extracts.

FCS is a technique that allows the measurement of diffusion constants of fluorophores, which allows then the estimation of their molecular weight (32). Whole cells synthesizing HpPex19p.GFP were broken, and membranes (P) were separated from the soluble fraction (S). The membrane fraction was subsequently solubilized by digitonin followed by centrifuga-

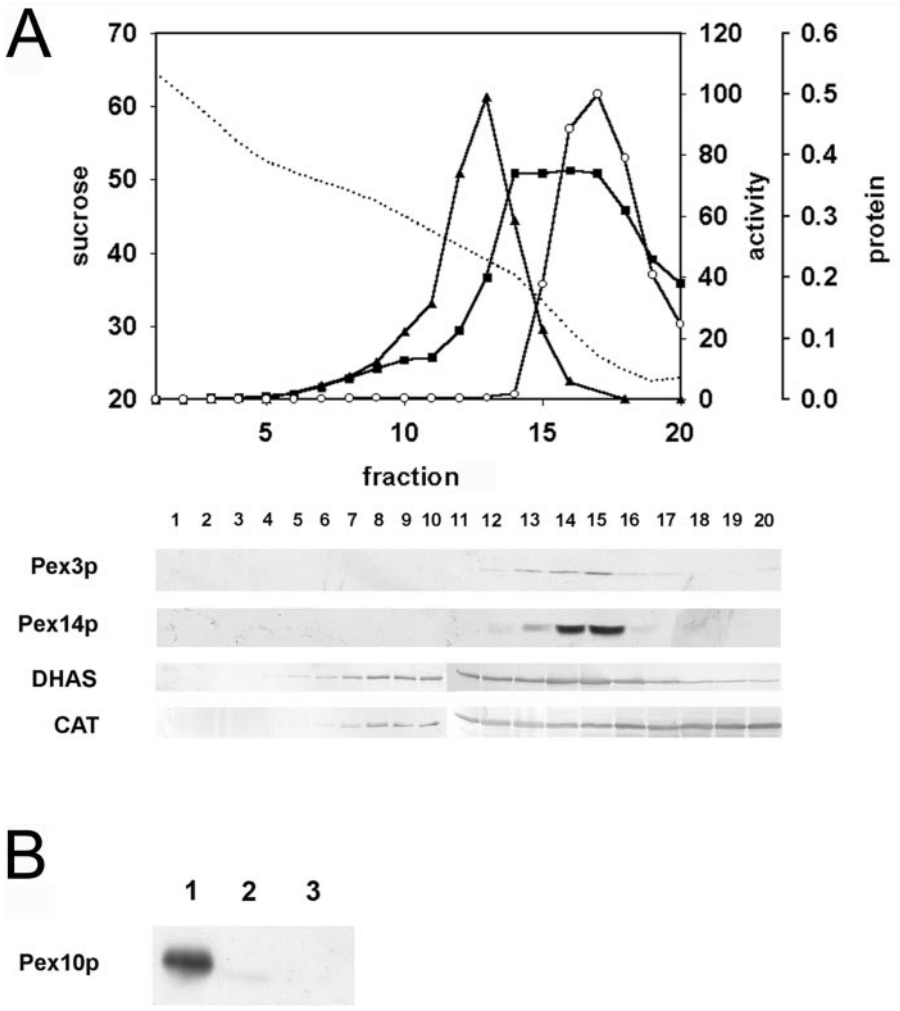

FIG. 6. **HpPex3p and HpPex14p colocalize at peroxisomal structures in Hp*pex19* cells producing Pex3p$_{N50}$-GFP.** *A*, a postnuclear supernatant prepared from homogenized, chemostat-grown *pex19*::P_{AOX}*PEX3*$_{N50}$*-GFP* cells was subjected to sucrose density centrifugation. The graph shows the protein (■) and sucrose concentrations (*dotted line*) as well as the activities of cytochrome *c* oxidase (▲) and AO (●). Protein concentrations are expressed as mg.ml^{-1}, sucrose concentrations as % (w/w), enzyme activities as percentages of the activity in the peak fractions, which were arbitrary set at 100. The fractions of the gradient were analyzed by Western blotting using the indicated antibodies. Equal portions of the fractions were loaded per lane. *B*, Western blots using crude cell extracts of WT (*lane 1*), Hp*pex19* cells (*lane 2*), and Hp*pex19*::P_{AOX}*PEX3*$_{N50}$*-GFP* (*lane 3*), showing the virtual absence of HpPex10p in the mutant cells.

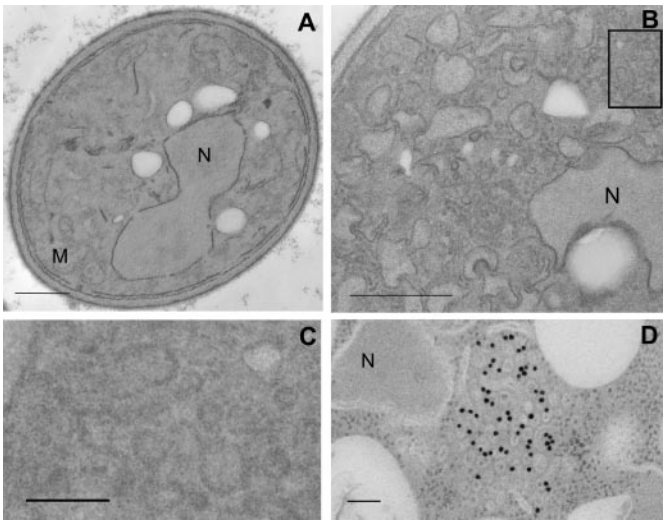

FIG. 7. **Morphological analysis of *S. cerevisiae pex19* cells overproducing ScPex3p.** In ultrathin sections of $KMnO_4$-fixed Sc*pex19* cells overproducing ScPex3p (Sc*pex19* plus pTF14) numerous small vesicular structures are visible in the cytosol (*B* and *C*), which were absent in Sc*pex19* control cells (*A*). *C* shows a magnification of the indicated region in *B*. Immunolabeling experiments using anti-ScPex3p antibodies revealed that these vesicles contained ScPex3p (*D*). The *bars* represent 0.5 μm (*A* and *B*) or 0.1 μm (*C* and *D*). *M*, mitochondrion; *N*, nucleus.

tion to remove insoluble material. P and S fractions obtained from cells lacking the HpPex19p.GFP fusion protein were used as controls. Normalized fluorescence autocorrelation curves of samples P and S were fitted globally to a diffusion model, including triplet kinetics (see "Experimental Procedures").

In fraction P (Fig. 10*A*), the best fit was achieved when a one-component diffusion model was used. Using the equation, $MW_1 = (\tau_1/\tau_2)^3 \times MW_2$, the molecular mass of the HpPex19p.GFP-containing complex was estimated to be 253 kDa (confidence limit, 206–360 kDa). Similar data were obtained when fraction S was analyzed by FCS (data not shown) and the size of this complex was similar (estimated molecular mass of ~243 kDa; confidence limits of 142–318 kDa). These data suggest that either HpPex19p may form homotetramers in both fractions (the calculated molecular mass of the HpPex19p.GFP fusion protein is 60 kDa) or alternatively, one or more proteins may be bound to a single HpPex19p-GFP molecule resulting in a protein complex with the total mass of ~250 kDa. In control samples prepared of cells that did not produce HpPex19.GFP, no fluorescence fluctuations that could be autocorrelated were observed.

Native gel electrophoresis experiments confirmed the presence of large HpPex19p.GFP-containing protein complexes in the P and S fractions. Upon Western blot analysis using anti-GFP antibodies, both in the P and S fractions the most dominant band was located ~250 kDa (Fig. 10*B*), which is in the same range as the size of the complexes predicted by FCS. In control cells lacking GFP, no cross-reacting bands were found, indicating that the observed bands are due to specific binding of the anti-GFP antibodies to the GFP fusion protein.

Although similar bands are found in both fractions, this is not due to contamination of the membrane fraction with solu-

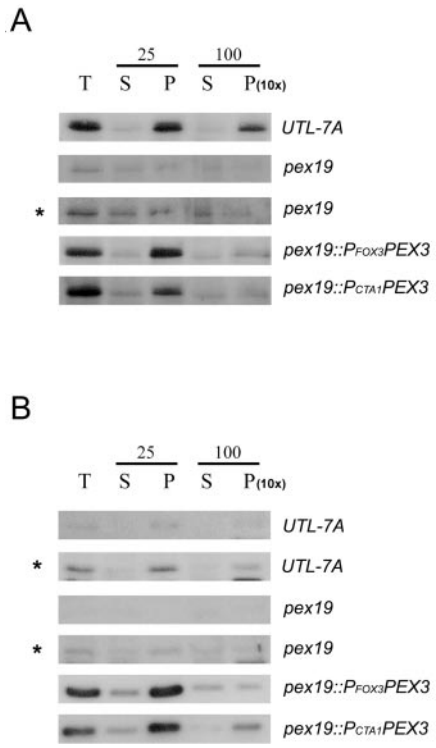

FIG. 8. **Overproduction of ScPex3p in *S. cerevisiae pex19* cells affects the protein level and sedimentation behavior of Pex13p.** Postnuclear supernatants (*T*) were prepared from oleic acid-induced cells of the indicated strains and subjected to differential centrifugation (two successive centrifugation steps at 25,000 × *g* (*25*) and 100,000 × *g* (*100*)). *S*, supernatant; *P*, pellet. All strains produced Protein A-tagged Pex13p. The fractions were analyzed by Western blotting using IgGs to decorate Protein A in the Pex13p-ProteinA fusion protein (*A*) or anti-Pex3p antibodies (*B*). Equal portions of each fraction were loaded per lane except for the 100,000 × *g* pellet fraction, of which 10 times more protein was loaded. *UTL-7A*, WT *S. cerevisiae*; *pTF14*, overexpression of *ScPEX3* under control of the FOX3 promoter; *pTF15*, overexpression of *ScPEX3* under control of the CTA1 promoter. *, prolonged exposure to visualize the protein bands.

ble proteins or *vice versa*. This is based on the results obtained with control blots, which revealed that the membrane marker protein HpPex3p was only detected in fraction P, whereas the soluble marker protein pyruvate carboxylase was confined to the soluble fraction (S; data not shown). Taken together, our data suggest that HpPex19p.GFP is predominantly present in protein complexes of ~250 kDa.

Fusion of an Myc tag or GFP to the C terminus of HpPex19p disables farnesylation at the C-terminal farnesylation site of the protein (-CKQT). Our finding that both fusion proteins are fully functional, therefore, indicates that HpPex19p farnesylation is not essential for peroxisome formation. This was confirmed by the observation that cells producing a mutant form of HpPex19p in which the farnesylation site is inactivated (*pex19*::P_{PEX19}*PEX19C286S*) also grew on methanol and formed peroxisomes (data not shown).

DISCUSSION

Here we report the cloning and characterization of the *H. polymorpha PEX19* gene. *PEX19* genes have been identified in several organisms, ranging from yeast to human, and encode hydrophilic proteins with a consensus sequence for farnesylation (1). A distinct role for Pex19p farnesylation has not been established yet. Also in *H. polymorpha* Pex19p we observed that farnesylation is not essential for its function in peroxisome biogenesis.

Fluorescence microscopy revealed that HpPex19p.GFP has a dual location and is present in the cytosol and at the peroxisome periphery. Similar observations have been made for other Pex19ps and led to the hypothesis that Pex19p may be a shuttling mPTS receptor by analogy to the receptors of peroxisomal matrix proteins, Pex5p and Pex7p (1).

Two-hybrid studies revealed that Pex19ps of various organisms interacted with multiple membrane proteins (4–5). Whether these interactions occur predominantly in the cytosol or at the peroxisomal membrane is still unclear. Human Pex19p (HsPex19p) has been shown to interact preferentially with newly synthesized PMPs in the cytosol, a finding that favors a function as mPTS receptor (3). However, by using fluorescence resonance energy transfer analysis, Muntau *et al.* (39) recently concluded that the interaction of HsPex3p and HsPex19p predominantly occurs at the peroxisomal membrane. Snyder *et al.* (4) reported that PpPex19p predominantly interacts with pre-existing PMPs at the peroxisomal membrane. At this location Pex19p may have a chaperone-like role for instance in facilitating PMP insertion/assembly.

Our native gel electrophoresis and FCS studies revealed that under steady-state conditions the bulk of the HpPex19p.GFP is present in relatively large protein complexes of ~250 kDa both in soluble and membrane-bound fractions. This seems to contradict the observation that Pex19ps interact with a large number of different PMPs, which would result in a range of Pex19p-PMP complexes of various sizes. However, these may be transient and, therefore, below the limit of detection.

Interestingly, an additional role for cytosolic rat Pex19p was proposed recently in internalization of a sodium-dependent phosphate co-transporter (40). Therefore, a portion of the cytosolic Pex19p in rat may function in another cellular process than peroxisome biogenesis, a phenomenon that deserves further attention in yeast research.

In most organisms studied so far, the levels of PMPs are strongly reduced in cells lacking Pex19p. In *S. cerevisiae pex19* cells the minor amounts of PMPs that remain are present in the cytosol, where they are rapidly degraded (7). Some PMPs are mislocalized to mitochondria in the absence of Pex19p (*e.g.* Pex14p in human fibroblasts (3)). Most likely these PMPs harbor cryptic sorting signals, which localize them to mitochondria when peroxisomal membranes are absent.

We show that the levels of HpPex3p and HpPex14p are not affected by the absence of HpPex19p in *H. polymorpha* cells, a finding that greatly facilitated the analysis of their location (HpPex3p, cytosol; HpPex14p, mitochondria). However, the level of HpPex10p was strongly reduced and below the level of detection.

In general, PMP mislocalization in peroxisome-deficient cells can be related to defects in their sorting or insertion/assembly machineries. Sorting defaults could, *e.g.*, result from improper mPTS recognition (*e.g.* due to a defect in the mPTS receptor). Also, the targeting mechanisms could still be functional, but not effective, because of defaults in PMP insertion/assembly (4, 8) or defects in the formation of the peroxisomal lipid bilayer.

In this report we showed that the absence of peroxisomal membranes and the mislocalization of PMPs in *H. polymorpha pex19* could be largely suppressed by overproduction of the first 50 amino acids of Pex3p fused to GFP ($Pex3_{N50}$.GFP) or full-length HpPex3p. In these cells peroxisomal structures were present that, based on biochemical and ultrastructural criteria, are peroxisomes and contained peroxisomal matrix and membrane proteins. These findings indicate that in the absence of HpPex19p PMPs apparently can be correctly sorted to peroxisomal membranes and the peroxisomal lipid bilayer can be formed. It is therefore unlikely that HpPex19p is the general mPTS receptor in *H. polymorpha*. Also, it is unlikely that

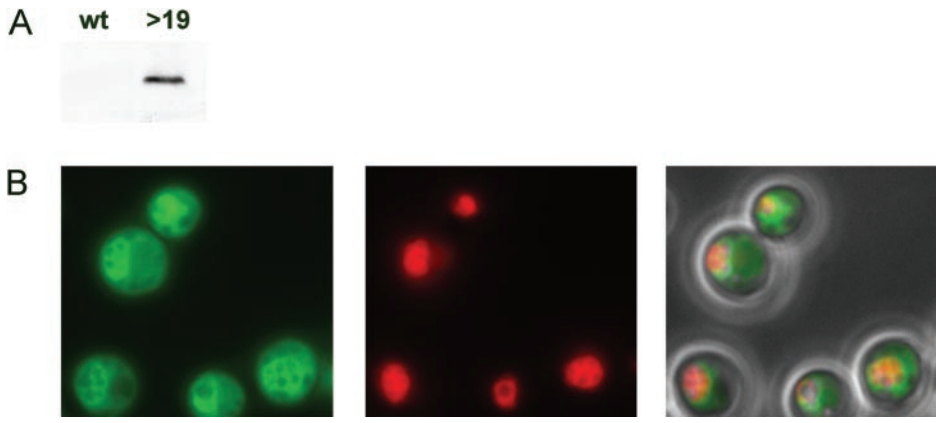

FIG. 9. **Localization of HpPex19p.** *A*, a Western blot decorated with anti-HpPex19p antibodies. Equal amounts of crude extracts of trichloroacetic acid-precipitated, methanol-grown cells were used. *WT*, wild type *H. polymorpha*; *>19*, Hp*pex19*::P_{PEX3}*Myc-PEX19*. Only in the blots of the latter strains was Pex19p visualized. *B*, fluorescence microscopy of cells that produce HpPex19p.GFP (*green fluorescence*, *left panel*). Fluorescence is evident in the cytosol and at the peroxisomal edges. DsRed-SKL is used to visualize peroxisomes (DsRed-SKL, *red fluorescence*, *middle panel*). The *right panel* shows an overlay of *bright-field*, *green fluorescence*, and *red fluorescence images*.

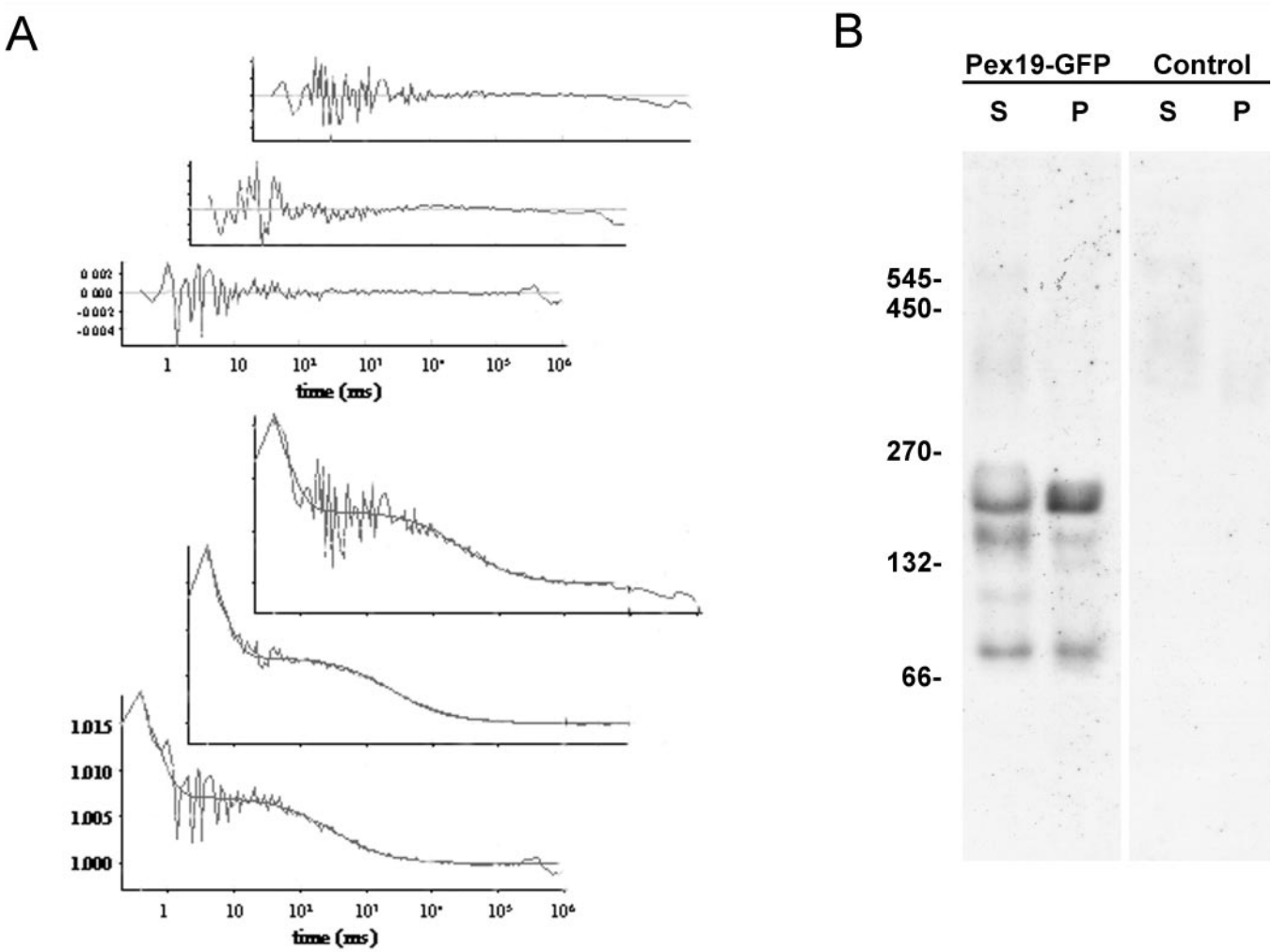

FIG. 10. **HpPex19p.GFP is present in large complexes, both in the cytosol and at the peroxisomal membrane.** *A*, examples of experimental autocorrelation curves, fitted curves, and residuals (*upper inset*) of FCS experiments using solubilized membrane fraction of whole cells producing HpPex19p.GFP. After global analysis of 20 experimental curves, a diffusion time of 243 μs was obtained (confidence limit: 226–272 μs). Based on these data the calculated molecular mass of the fluorescent protein complex is estimated to amount 253 kDa (confidence limit: 206–360 kDa) assuming that the complex is globular in shape. *B*, a Western blot of a native gel loaded with solubilized membrane (*P*) or soluble fraction (*S*) of the same cells (Pex19-GFP) or controls cells that do not produce Pex19-GFP (control). The blots were decorated with anti-GFP antibodies. Both fractions contain a dominant band with an apparent molecular mass of ~250 kDa.

HpPex19p is essential for the formation of the peroxisomal lipid bilayer.

The peroxisomal structures that are formed in Hp*pex19* cells producing $Pex3_{N50}$.GFP contain a significant portion of the major matrix proteins. Therefore the membranes of these organelles apparently contain some functional protein complexes

able to facilitate matrix protein import. This observation does not exclude a function for HpPex19p in the efficient formation of functional PMP complexes. Possibly, in the absence of HpPex19p non-functional PMP complexes exist, which may explain why peroxisome formation and matrix protein import is not fully restored. Indeed, the level of HpPex10p remained extremely low in these cells, which may be one of the reasons for the partial import defect of the major matrix proteins and the complete defect of catalase import.

Also in *Y. lipolytica pex19* cells, which still contain peroxisomal structures, the levels of both PMPs tested (YlPex2p and YlPex16p) were significantly reduced compared with WT cells (8). This suggests that, in this organism also, PMPs are still correctly targeted to peroxisomal membranes but failed to produce fully functional protein complexes (*e.g.* those involved in matrix protein import (41, 42)), a phenomenon that may be related to the fact that YlPex2p and YlPex16p are instable.

A similar reasoning may explain why in Sc*pex19* cells that overproduce ScPex3p matrix protein import are not restored. Nevertheless, in these cells membranes are formed that contain ScPex3p and ScPex13p. In conclusion, our data are consistent with a role of Pex19ps in the formation of functional membrane protein complexes rather than in PMP sorting or formation of the peroxisomal lipid bilayer.

A specific characteristic of cells defective in Pex19p is that their respective peroxisome phenotypes differ strongly, varying from the complete absence of peroxisome structures (*e.g.* in mammalian cells and *S. cerevisiae*) to the presence of normal peroxisomal structures (in *Y. lipolytica*). Our data in *H. polymorpha* may add to an explanation of these puzzling differences. Obviously, one option is that these differences are related to specific species differences. However, in *H. polymorpha pex19*, we can largely mimic the various above phenotypes by controlling the levels of HpPex3p, ranging from complete absence of peroxisomes (normal HpPex3p levels) to the presence of peroxisomes (HpPex3p or $Pex3N_{50}$.GFP overproduction).

Previous data from Faber *et al.* (20) demonstrated that small peroxisomal vesicles can be formed from the nuclear envelope in Hp*pex3* cells upon synthesis of $Pex3_{N50}$.GFP, structures that can develop into normal peroxisomes. Comparable observations have been made in *Y. lipolytica* (43). We showed that a comparable process also occurred with *H. polymorpha* in the absence of HpPex19p and resulted in the formation of peroxisomes in Hp*pex19* cells. Based on these observations we hypothesize that peroxisome formation from the endomembrane system is almost completely blocked in *S. cerevisiae*, *H. polymorpha*, and mammalian cells defective in Pex19p but regularly occurring in *Y. lipolytica pex19*. An intermediate situation is observed in *P. pastoris*, which contains small vesicular structures in the absence of Pex19p. We speculate that the absence or presence of peroxisomal structures may be related to futile differences in PMP and/or peroxin levels, differences that may even be related to changes in cultivation conditions or, in higher eukaryotes, dependent on tissue and developmental stage (44). These minor differences may explain why in certain organisms the peroxisomal structures are absent in the absence of Pex19p, but readily detectable in others.

Acknowledgments—The skillful assistance of Arjen Krikken, Klaas Sjollema, and Patricia Stevens in various parts of this study is gratefully acknowledged. We thank Dr. S. Subramani for providing us with the *P. pastoris pex19* (SKF13) strain, Dr. M. Komori for the plasmid pHIPX10-PEX14eGFP, and Dr. B. S. Glick for the plasmid-containing DsRed-T1.

REFERENCES

1. Purdue, P. E., and Lazarow, P. B. (2001) *Annu. Rev. Cell Dev. Biol.* **17,** 701–752
2. Snyder, W. B., Faber, K. N., Wenzel, T. J., Koller, A., Luers, G. H., Rangell, L., Keller, G. A., and Subramani, S. (1999) *Mol. Biol. Cell* **10,** 1745–1761
3. Sacksteder, K. A., Jones, J. M., South, S. T., Li, X., Liu, Y., and Gould, S. J. (2000) *J. Cell Biol.* **148,** 931–944
4. Snyder, W. B., Koller, A., Choy, A. J., and Subramani, S. (2000) *J. Cell Biol.* **149,** 1171–1178
5. Fransen, M., Wylin, T., Brees, C., Mannaerts, G. P., and van Veldhoven, P. P. (2001) *Mol. Cell. Biol.* **21,** 4413–4424
6. Götte, K., Girzalsky, W., Linkert, M., Baumgart, E., Kammerer, S., Kunau, W. H., and Erdmann, R. (1998) *Mol. Cell. Biol.* **18,** 616–628
7. Hettema, E. H., Girzalsky, W., van den Berg, M., Erdmann, R., and Distel, B. (2000) *EMBO J.* **19,** 223–233
8. Lambkin, G. R., and Rachubinski, R. A. (2001) *Mol. Biol. Cell* **12,** 3353–3364
9. Van Dijken, J. P., Otto, R., and Harder, W. (1976) *Arch. Microbiol.* **111,** 137–144
10. Sambrook, J., Fritsch, E. F., and Maniatis, T. (1989) *Molecular Cloning: A Laboratory Manual*, Cold Spring Harbor Laboratory Press, Cold Spring Harbor, NY
11. Baerends, R. J. S., Rasmussen, S. W., Hilbrands, R. E., van der Heide, M., Faber, K. N., Reuvekamp, P. T., Kiel, J. A. K. W., Cregg, J. M., van der Klei, I. J., and Veenhuis, M. (1996) *J. Biol. Chem.* **271,** 8887–8894
12. Faber, K. N., Swaving, G. J., Faber, F., Ab, G., Harder, W., Veenhuis, M., and Haima, P. (1992) *J. Gen. Microbiol.* **138,** 2405–2416
13. Faber, K. N., Haima, P., Harder, W., Veenhuis, M., and Ab, G. (1994) *Curr. Genet.* **25,** 305–310
14. Kiel, J. A. K. W., Keizer-Gunnink, I., Krause, T., Komori, M., and Veenhuis, M. (1995) *FEBS Lett.* **377,** 434–438
15. Haan, G. J., Faber, K. N., Baerends, R. J., Koek, A., Krikken, A., Kiel, J. A. K. W., van der Klei, I. J., and Veenhuis, M. (2002) *J. Biol. Chem.* **277,** 26609–26617
16. Shen, S., Sulter, G., Jeffries, T. W., and Cregg, J. M. (1998) *Gene* (*Amst.*) **216,** 93–102
17. Altschul, S. F., Gish, W., Miller, W., Myers, E. W., and Lipman, D. J. (1990) *J. Mol. Biol.* **215,** 403–410
18. Merckelbach, A., Godecke, S., Janowicz, Z. A., and Hollenberg, C. P. (1993) *Appl. Microbiol. Biotechnol.* **40,** 361–364
19. Baerends, R. J. S., Faber, K. N., Kram, A. M., Kiel, J. A. K. W., van der Klei, I. J., and Veenhuis, M. (2000) *J. Biol. Chem.* **275,** 9986–9995
20. Faber, K. N., Haan, G. J., Baerends, R. J. S., Kram, A. M., and Veenhuis, M. (2002) *J. Biol. Chem.* **277,** 11026–11033
21. Gietl, C., Faber, K. N., van der Klei, I. J., and Veenhuis, M. (1994) *Proc. Natl. Acad. Sci. U. S. A.* **91,** 3151–3155
22. Leao-Helder, A. N., Krikken, A. M., Van der Klei, I. J., Kiel, J. A. K. W., and Veenhuis, M. (2003) *J. Biol. Chem.* **278,** 40749–40756
23. Bevis, B. J., and Glick, B. S. (2002) *Nat. Biotechnol.* **20,** 83–87
24. Knop, M., Siegers, K., Pereira, G., Zachariae, W., Winsor, B., Nasmyth, K., and Schiebel, E. (1999) *Yeast* **15,** 963–972
25. van der Klei, I. J., van der Heide, M., Baerends, R. J. S., Rechinger, K. B., Nicolay, K., Kiel, J. A. K. W., and Veenhuis, M. (1998) *Curr. Genet.* **34,** 1–11
26. Goodman, J. M., Maher, J., Silver, P. A., Pacifico, A., and Sanders, D. (1986) *J. Biol. Chem.* **261,** 3464–3468
27. Verduyn, C., Van Dijken, J. P., and Scheffers, W. A. (1984) *J. Microbiol. Methods* **2,** 15–25
28. Douma, A. C., Veenhuis, M., de Koning, W., Evers, M. E., and Harder, W. (1985) *Arch. Microbiol.* **143,** 237–243
29. Laemmli, U. K. (1970) *Nature* **227,** 680–685
30. Musgrove, J. E., Johnson, R. A., and Ellis, R. J. (1987) *Eur. J. Biochem.* **163,** 529–534
31. Kyhse-Andersen, J. (1984) *J. Biochem. Biophys. Methods* **10,** 203–209
32. Wang, D., Visser, N. V., Veenhuis, M., and van der Klei, I. J. (2003) *J. Biol. Chem.* **278,** 43340–43345
33. Widengren, J., Mets, U., and Rigler, R. (1995) *J. Phys. Chem.* **99,** 13368–13379
34. Beechem, J. M., Gratton, E., Ameloot, M., Knutson, J. R., and Brand, L. (1991) in *Topics in Fluorescence Spectroscopy* (Lakowicz, J. R., eds) p. 241, Plenum Press, New York
35. Waterham, H. R., Titorenko, V. I., Haima, P., Cregg, J. M., Harder, W., and Veenhuis, M. (1994) *J. Cell Biol.* **127,** 737–749
36. Cregg, J. M., van der Klei, I. J., Sulter, G. J., Veenhuis, M., and Harder, W. (1990) *Yeast* **6,** 87–97
37. Zwart, K. B., Veenhuis, M., and Harder, W. (1983) *Antonie Van Leeuwenhoek* **49,** 369–385
38. Hock, B., and Gietl, C. (1982) *Ann. N. Y. Acad. Sci.* **386,** 350–376
39. Muntau, A. C., Roscher, A. A., Kunau, W. H., and Dodt, G. (2003) *Eur. J. Cell Biol.* **82,** 333–342
40. Ito, M., Iidawa, S., Izuka, M., Haito, S., Segawa, H., Kuwahata, M., Ohkido, I., Ohno, H., and Miyamoto, K. I. (2004) *Biochem. J.* **377,** 607–616
41. Hazra, P. P., Suriapranata, I., Snyder, W. B., and Subramani, S. (2002) *Traffic* **3,** 560–574
42. Agne, B., Meindl, N. M., Niederhoff, K., Einwachter, H., Rehling, P., Sickmann, A., Meyer, H. E., Girzalsky, W., and Kunau, W. H. (2003) *Mol. Cell* **11,** 635–646
43. Bascom, R. A., Chan, H., and Rachubinski, R. A. (2003) *Mol. Biol. Cell* **14,** 939–957
44. Geuze, H. J., Murk, J. L., Stroobants, A. K., Griffith, J. M., Kleijmeer, M. J., Koster, A. J., Verkleij, A. J., Distel, B., and Tabak, H. F. (2003) *Mol. Biol. Cell* **14,** 2900–2907
45. Gleeson, M. A. G., and Sudbery, P. E. (1988) *Yeast* **4,** 293–303
46. Erdmann, R., Veenhuis, M., Mertens, D., and Kunau, W. H. (1989) *Proc. Natl. Acad. Sci. U. S. A.* **86,** 5419–5423